

Electronic Supplementary Information

Ratiometric sensing of lysine through the formation of pyrene excimer: Experimental and computational studies

Sisir Lohar,^a Damir A. Safin,^b Archya Sengupta,^c Ansuman Chattopadhyay,^c Jesús Sanmartín Matalobos,^d Maria G. Babashkina,^{*b} Koen Robeyns,^b Mariusz P. Mitoraj,^{*e} Piotr Kubisiak,^e Yann Garcia,^{*b} and Debasis Das^{*a}

^aDepartment of Chemistry, The University of Burdwan, 713104, Burdwan, West Bengal, India. Fax: (+91) 342 2530452; Tel: (+91) 342 2533913; E-mail: ddas100in@yahoo.com

^bInstitute of Condensed Matter and Nanosciences, Molecules, Solids and Reactivity (IMCN/MOST), Université Catholique de Louvain, Place L. Pasteur 1, 1348 Louvain-la-Neuve, Belgium. Fax: +32(0) 1047 2330; Tel: +32(0) 1047 2831; E-mail: maria.babashkina@gmail.com

^cDepartment of Zoology, Visva Bharati University, Santiniketan, West Bengal, India.

^dDepartamento de Química Inorgánica, Facultade de Química, Avda. Das Ciencias s/n, 15782, Santiago de Compostela, Spain.

^eDepartment of Theoretical Chemistry, Faculty of Chemistry, Jagiellonian University, R. Ingardena 3, 30-060 Cracow, Poland. E-mail: mitoraj@chemia.uj.edu.pl

Materials and methods. High-purity HEPES, pyrene-1-carbaldehyde, benzylamine, picolyl amine, *n*-butylamine, thiophene methyl amine, anthracene-9-carboxaldehyde and naphthalene-1-carbaldehyde were purchased from Sigma Aldrich (India). Amino acids were purchased from Merck (India). Solvents were of spectroscopic grade. Other chemicals were of analytical reagent grade and had been used without further purification except when specified. Mili-Q Milipore 18.2 MΩ cm⁻¹ water has been used throughout all the experiments. A JASCO (model V-570) UV-vis. spectrophotometer was used for recording absorption spectra. FTIR spectra were recorded on a JASCO FTIR-H20 spectrophotometer. Mass spectra were performed on a QTOF Micro YA 263 mass spectrometer in the ES positive mode. ¹H NMR spectra in CDCl₃ were recorded using a Bruker Avance 500 (500 MHz). ¹H NMR titration in CD₃OD was recorded using a Bruker Avance 600 (600 MHz). pH measurements were performed with a Systronics digital pH meter (model 335). All spectra were recorded at room temperature except fluorescence microscope images. Elemental analyses were performed on a Perkin Elmer 2400 CHN analyzer.

UV-vis and fluorescence titration. The path length of cells used for absorption and emission studies was 1 cm. For UV-vis and fluorescence titrations, stock solutions of **BAPA**, **PAPA**, **NBAPA**, **PTA**, **BAACA** and **BANA** (10 μM) were prepared in HEPES buffered (0.1 M; MeOH:H₂O, 1:1 v/v; pH 7.4). Working solutions of **APA**, **PAPA**, **NBAPA**, **PTA**, **BAACA**, **BANA** and lysine were prepared from their respective stock solutions. Fluorescence measurements were performed using 5 nm × 5 nm slit width.

Determination of the detection limit. Fluorescence titration of **BAPA** with lysine was carried out by adding aliquots of the micromolar concentration of lysine. From the concentration at which there was a sharp change in the fluorescence intensity multiplied by the concentration of **BAPA** gave the detection limit. The following equation was applied to calculate the detection limit:

$$DL = CL \times CT,$$

where DL is the detection limit, CL is the concentration of **BAPA**, CT is the concentration of lysine at which fluorescence enhanced with the signal-over-noise ratio equal to three sigma.

$$\text{Thus, } DL = 10 \mu\text{M} \times 0.005 \mu\text{M} = 0.05 \mu\text{M} = 5 \times 10^{-8} \text{ M.}$$

In vitro cell imaging. Human breast cancer cell line MCF7 was grown in DMEM (Sigma, St. Louis, USA) supplemented with 10% fetal bovine serum (Sigma, St. Louis, USA), 2 mM glutamine, 100 U m/L penicillin-streptomycin solution (Gibco, Invitrogen, USA) in the presence of 5% CO₂ at 37 °C. For *in vitro* imaging studies, cells were seeded in 6 well culture plates with a seeding density of 10⁵ cells per well. After reaching 60–70% confluence, the previous media was replaced with serum free media, supplemented by lysine and **BAPA** at 50 μM and 20 μM, and incubated for 2 h to facilitate the metal ion or **BAPA** uptake by the cells. Then the cells were placed under an inverted microscope (Dewinter, Italy) at different magnifications to examine any adverse effect on cellular morphology. **BAPA** treated cells were then incubated with lysine for 15–30 min and observed under an inverted fluorescence microscope at different magnifications with a blue filter. Images were taken through an attached ccd camera with the help of Bio-Wizard 4.2 software. A control experiment was done using medium devoid of lysine.

Density Functional Theory (DFT) based calculations. We have applied in the ADF/DFT¹ ground state optimizations the BLYP-D3/TZ2P protocol. For the TD-DFT excited state optimization (S₁) of **BAPA** monomer the B3LYP, as implemented in the Gaussian 09 package,² was applied. Similarly, the absorption spectra from ADF were generated based on B3LYP/TZP. Deformation density contributions of the ETS-NOCV method were plotted based on the ADF-GUI interface.³

ETS-NOCV bonding analysis. Historically the Natural Orbitals for Chemical Valence (NOCV) have been derived from the Nalewajski-Mrozek valence theory as eigenvectors that diagonalizes the deformation density matrix. It was shown that the natural orbitals for chemical valence pairs (ψ_{-k}, ψ_k) decompose the differential density $\Delta\rho$ into NOCV-contributions ($\Delta\rho_k$):

$$\Delta\rho(r) = \sum_{k=1}^{M/2} \nu_k [-\psi_{-k}^2(r) + \psi_k^2(r)] = \sum_{k=1}^{M/2} \Delta\rho_k(r),$$

where ν_k and M stand for the NOCV eigenvalues and the number of basis functions, respectively. Visual inspection of deformation density plots ($\Delta\rho_k$) helps to attribute symmetry and the direction of the charge flow. In addition,

these pictures are enriched by providing the energetic estimations, $\Delta E_{orb}(k)$, for each $\Delta\rho_k$ within ETS-NOCV scheme. The exact formula, which links the ETS and NOCV methods, will be given in the next paragraph, after we briefly present the basic concept of ETS scheme. In this method the total bonding energy ΔE_{total} between interacting fragments, exhibiting the geometry as in the combined complex, is divided into the three components: $\Delta E_{total} = \Delta E_{elstat} + \Delta E_{Pauli} + \Delta E_{orb}$. The first term, ΔE_{elstat} , corresponds to the classical electrostatic interaction between the promoted fragments as they are brought to their positions in the final complex. The second term, ΔE_{Pauli} , accounts for the repulsive Pauli interaction between occupied orbitals on the two fragments in the combined molecule. Finally, the last stabilizing term, ΔE_{orb} represents the interactions between the occupied molecular orbitals of one fragment with the unoccupied molecular orbitals of the other fragment as well as mixing of occupied and virtual orbitals within the same fragment (inner-fragment polarization). This energy term may be linked to the electronic bonding effect coming from the formation of a chemical bond. The three last terms (ΔE_{elstat} , ΔE_{Pauli} , ΔE_{orb}) very often are combined into the instantaneous interaction energy, ΔE_{int} , as it describes the interaction between the fragments in the geometry of the complex.

In the combined ETS-NOCV scheme the orbital interaction term (ΔE_{orb}) is expressed in terms of NOCV's eigenvalues (v_k) as:

$$\Delta E_{orb} = \sum_k \Delta E_{orb}(k) = \sum_{k=1}^{M/2} v_k [-F_{-k,-k}^{TS} + F_{k,k}^{TS}],$$

where $F_{i,i}^{TS}$ are diagonal Kohn-Sham matrix elements defined over NOCV with respect to the transition state (TS) density (at the midpoint between density of the molecule and the sum of fragment densities). The above components $\Delta E_{orb}(k)$ provide the energetic estimation of $\Delta\rho_k$ that may be related to the importance of a particular electron flow channel for the bonding between the considered molecular fragments. ETS-NOCV analysis was done based on the Amsterdam Density Functional (ADF) package in which this scheme was implemented.

Synthesis of (E)-1-phenyl-N-(pyren-1-ylmethylene)methanamine (BAPA). BAPA was synthesized by the condensation of pyrene 1-carboxaldehyde (250 mg, 1.09 mmol) with benzylamine (116 mg, 1.09 mmol) in dry MeOH (20 mL) followed by reflux for 6 h. Light yellow crystals were formed upon slow evaporation of the solvent. Yield: 320 mg (92%). $^1\text{H NMR}$, δ : 5.07 (s, 2H, CH_2), 7.31 (t, $^3J_{\text{H,H}} = 7.3$ Hz, 1H, *p*-H, Ph), 7.41 (t, $^3J_{\text{H,H}} = 7.2$ Hz, 2H, *m*-H, Ph), 7.49 (d, $^3J_{\text{H,H}} = 7.2$ Hz, 2H, *o*-H, Ph), 8.00–8.27 (m, 7H, pyrene), 8.61 (d, $^3J_{\text{H,H}} = 8.1$ Hz, 1H, pyrene), 8.97 (d, $^3J_{\text{H,H}} = 8.1$ Hz, 1H, pyrene), 9.44 (s, 1H, $\text{CH}=\text{N}$) ppm. *Anal.* Calcd. for $\text{C}_{24}\text{H}_{17}\text{N}$ (319.41): C 90.25, H 5.36, N 4.39. Found: C 90.37, H 5.41, N 4.30%.

Synthesis of (E)-N-(pyren-1-ylmethylene)-1-(pyridin-2-yl)methanamine (PAPA). PAPA was synthesized in a similar way as BAPA but using a methanolic solution of 2-(2-aminomethyl)pyridine (118 mg, 1.09 mmol) instead of benzylamine. The crude product, obtained after distillation of the solvent, was purified by column chromatography using hexane/ethyl acetate yielding light yellow solid. Yield: 0.262g (75%). $^1\text{H NMR}$, δ : 5.25 (s,

2H, CH₂), 7.32 (t, ³J_{H,H} = 7.7 Hz, 1H, Py), 7.40 (d, ³J_{H,H} = 7.7 Hz, 1H, Py), 7.56 (t, ³J_{H,H} = 7.8 Hz, 1H, Py), 8.08–8.37 (m, 7H, pyrene), 8.42 (d, ³J_{H,H} = 7.8 Hz, 1H, Py), 8.69 (d, ³J_{H,H} = 8.1 Hz, 1H, pyrene), 9.05 (d, ³J_{H,H} = 8.1 Hz, 1H, pyrene), 9.52 (s, 1H, CH=N) ppm. *Anal.* Calcd. for C₂₃H₁₆N₂ (320.39): C 86.22, H 5.03, N 8.74. Found: C 86.08, H 5.09, N 8.65%.

Synthesis of (*E*)-N-(pyren-1-ylmethylene)butan-1-amine (NBAPA). NBAPA was synthesized in a similar way as BAPA but using a methanolic solution of *n*-butylamine (80 mg, 1.09 mmol) instead of benzylamine. Light yellow crystals were formed upon slow evaporation of the solvent. Yield: 0.290 g (94%). ¹H NMR, δ : 1.03 (t, ³J_{H,H} = 7.4 Hz, 3H, CH₃), 1.53 (sextuplet, ³J_{H,H} = 7.4 Hz, 2H, CH₂), 1.85 (quintuplet, ³J_{H,H} = 7.3 Hz, 2H, CH₂), 3.85 (t, ³J_{H,H} = 7.1 Hz, 2H, CH₂), 7.72–8.03 (m, 7H, pyrene), 8.34 (d, ³J_{H,H} = 8.2 Hz, 1H, pyrene), 8.70 (d, ³J_{H,H} = 8.2 Hz, 1H, pyrene), 9.17 (s, 1H, CH=N) ppm. *Anal.* Calcd. for C₂₁H₁₉N (285.39): C 88.38, H 6.71, N 4.91. Found: C 88.53, H 6.59, N 4.85%.

Synthesis of (*E*)-N-(pyren-1-ylmethylene)-1-(thiophen-2-yl)methanamine (PTA). PTA was prepared described in the literature.⁴ *Anal.* Calcd. for C₂₂H₁₅NS (325.43): C 81.20, H 4.65, N 4.30. Found: C 81.11, H 4.72, N 4.23%.

Synthesis of (*Z*)-N-(anthracen-9-ylmethylene)-1-phenylmethanamine (BAACA). BAACA was synthesized by the condensation of anthracene-9-carboxaldehyde (250 mg, 1.12 mmol) with benzylamine (130 mg, 1.12 mmol) in dry MeOH (20 mL) followed by reflux for 6 h. Colorless crystals were formed upon slow evaporation of the solvent. Yield: 330 mg (92%). ¹H NMR, δ : 5.16 (s, 2H, CH₂), 7.17–7.61 (m, 8H, Ph + anthracene), 8.02 (d, ³J_{H,H} = 6.8 Hz, 2H, anthracene), 8.52 (d, ³J_{H,H} = 6.8 Hz, 2H, anthracene), 8.56 (s, 1H, anthracene), 9.57 (s, 1H, CH=N) ppm. *Anal.* Calcd. for C₂₂H₁₇N (295.38): C 89.46, H 5.80, N 4.74. Found: C 89.62, H 5.91, N 4.82%.

Synthesis of (*Z*)-N-(naphthalen-1-ylmethylene)-1-phenylmethanamine (BANA). BANA was synthesized in a similar way as BAACA but using a methanolic solution of 1-naphthaldehyde (175 mg, 1.12 mmol) instead of anthracene-9-carboxaldehyde. Light yellow solid was formed upon slow evaporation of the solvent. Yield: 260 mg (91%). ¹H NMR, δ : 4.97 (s, 2H, CH₂), 7.27–7.67 (m, 7H, Ph + naphthalene), 7.85–7.99 (m, 4H, naphthalene), 8.97 (d, ³J_{H,H} = 8.5 Hz, 1H, naphthalene), 9.07 (s, 1H, CH=N) ppm. *Anal.* Calcd. for C₁₈H₁₅N (245.32): C 88.13, H 6.16, N 5.71. Found: C 87.98, H 6.08, N 5.64%.

X-ray crystallography. The X-ray data for BAPA were collected at 150(2) K on a Mar345 image plate detector using Mo-K α radiation (Xenocs Fox3D mirror). The data were integrated with the crysAlisPro software.⁵ The implemented empirical absorption correction was applied. The structure was solved by direct methods using the SHELXS-97 program.⁶ C₂₄H₁₇N, *M*_r = 319.39 g mol⁻¹, monoclinic, space group *P*2₁/*c*, *a* = 13.0849(4), *b* =

9.1297(2), $c = 13.5767(4)$ Å, $\beta = 93.893(3)^\circ$, $V = 1618.15(8)$ Å³, $Z = 4$, $\rho = 1.311$ g cm⁻³, μ (Mo-K α) = 0.076 mm⁻¹, reflections: 10334 collected, 2953 unique, $R_{\text{int}} = 0.050$, $R_1(\text{all}) = 0.0708$, $wR_2(\text{all}) = 0.1199$.

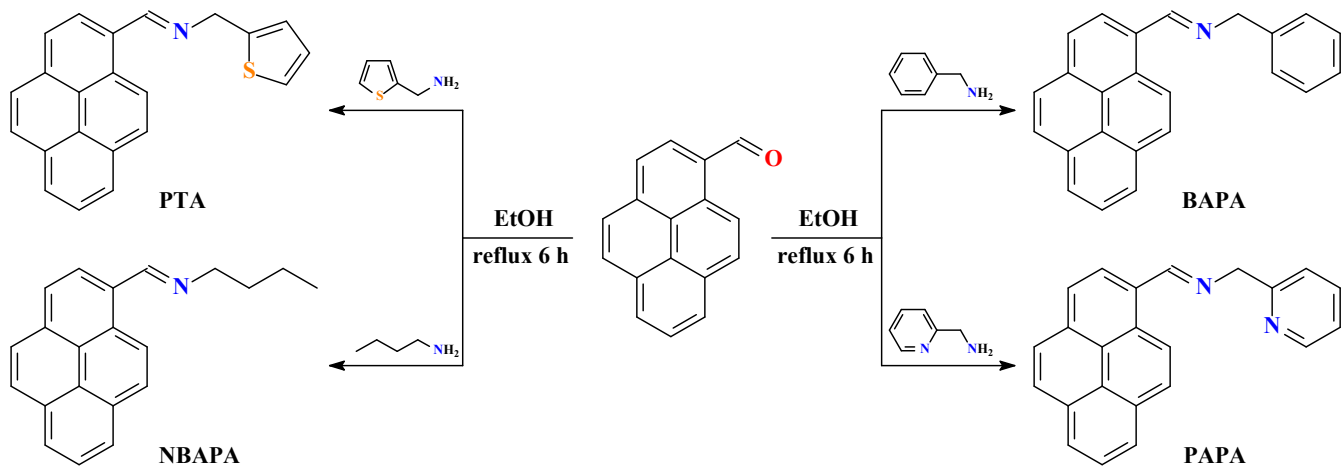
The X-ray data for **BAACA** were collected at 100(2) K on a Bruker X8 kappa APEXII CCD using Mo-K α radiation (graphite monochromator). The Apex2 software was used to integrate the data and SADABS was used for the absorption correction. The structure was solved by SIR97.⁷ C₂₂ H₁₇ N, $M_r = 295.37$ g mol⁻¹, monoclinic, space group $P2_1/n$, $a = 4.2713(12)$, $b = 14.110(4)$, $c = 25.725(7)$ Å, $\beta = 91.832(5)^\circ$, $V = 1549.6(7)$ Å³, $Z = 4$, $\rho = 1.266$ g cm⁻³, μ (Mo-K α) = 0.073 mm⁻¹, reflections: 19560 collected, 3570 unique, $R_{\text{int}} = 0.0565$, $R_1(\text{all}) = 0.071$, $wR_2(\text{all}) = 0.12$.

Both structures were refined by full-matrix least squares on $|F^2|$ using SHELXL-97.⁶ Non-hydrogen atoms were anisotropically refined and the hydrogen atoms were placed on calculated positions in riding mode with temperature factors fixed at 1.2 times U_{eq} of the parent atoms. Figures were generated using the program Mercury.⁸ CCDC 931269 (**BAPA**) and 938292 (**BAACA**) contains the supplementary crystallographic data. These data can be obtained free of charge via <http://www.ccdc.cam.ac.uk/conts/retrieving.html>, or from the Cambridge Crystallographic Data Centre, 12 Union Road, Cambridge CB2 1EZ, UK; fax: (+44) 1223-336-033; or e-mail: deposit@ccdc.cam.ac.uk.

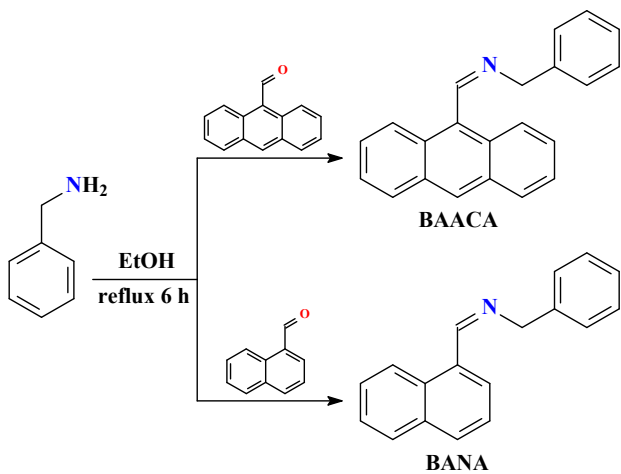
References

- 1 a) G. te Velde, F. M. Bickelhaupt, E. J. Baerends, C. Fonseca Guerra, S. J. A. van Gisbergen, J. G. Snijders and T. Ziegler, *J. Comput. Chem.*, 2001, **22**, 931 and references therein; b) E. J. Baerends, J. Autschbach, D. Bashford, A. Bérces, F. M. Bickelhaupt, C. Bo, P. M. Boerrigter, L. Cavallo, D. P. Chong, L. Deng, R. M. Dickson, D. E. Ellis, M. van Faassen, L. Fan, T. H. Fischer, C. Fonseca Guerra, A. Ghysels, A. Giammona, S. J. A. van Gisbergen, A. W. Götz, J. A. Groeneveld, O. V. Gritsenko, M. Grüning, F. E. Harris, P. van den Hoek, C. R. Jacob, H. Jacobsen, L. Jensen, G. van Kessel, F. Kootstra, M. V. Krykunov, E. van Lenthe, D. A. McCormack, A. Michalak, M. Mitoraj, J. Neugebauer, V. P. Nicu, L. Noodleman, V. P. Osinga, S. Patchkovskii, P. H. T. Philipsen, D. Post, C. C. Pye, W. Ravenek, J. I. Rodríguez, P. Ros, P. R. T. Schipper, G. Schreckenbach, M. Seth, J. G. Snijders, M. Solà, M. Swart, D. Swerhone, G. te Velde, P. Vernooijs, L. Versluis, L. Visscher, O. Visser, F. Wang, T. A. Wesolowski, E. M. van Wezenbeek, G. Wiesenekker, S. K. Wolff, T. K. Woo, A. L. Yakovlev and T. Ziegler, Theoretical Chemistry, Vrije Universiteit: Amsterdam.
- 2 M. J. Frisch, G. W. Trucks, H. B. Schlegel, G. E. Scuseria, M. A. Robb, J. R. Cheeseman, G. Scalmani, V. Barone, B. Mennucci, G. A. Petersson, H. Nakatsuji, M. Caricato, X. Li, H. P. Hratchian, A. F. Izmaylov, J. Bloino, G. Zheng, J. L. Sonnenberg, M. Hada, M. Ehara, K. Toyota, R. Fukuda, J. Hasegawa, M. Ishida, T.

- Nakajima, Y. Honda, O. Kitao, H. Nakai, T. Vreven, J. A. Montgomery Jr., J. E. Peralta, F. Ogliaro, M. Bearpark, J. J. Heyd, E. Brothers, K. N. Kudin, V. N. Staroverov, R. Kobayashi, J. Normand, K. Raghavachari, A. Rendell, J. C. Burant, S. S. Iyengar, J. Tomasi, M. Cossi, N. Rega, J. M. Millam, M. Klene, J. E. Knox, J. B. Cross, V. Bakken, C. Adamo, J. Jaramillo, R. Gomperts, R. E. Stratmann, O. Yazyev, A. J. Austin, R. Cammi, C. Pomelli, J. W. Ochterski, R. L. Martin, K. Morokuma, V. G. Zakrzewski, G. A. Voth, P. Salvador, J. J. Dannenberg, S. Dapprich, A. D. Daniels, Ö. Farkas, J. B. Foresman, J. V. Ortiz, J. Cioslowski and D. J. Fox, Gaussian 09, Gaussian Inc., Wallingford CT, 2009.
- 3 O. Visser, P. Leyronnas, W. J. van Zeist and M. Lupki, ADF-GUI 2012.01, SCM, Amsterdam, The Netherlands, <http://www.scm.com>.
- 4 A. Banerjee, A. Sahana, S. Das, S. Lohar, B. Sarkar, S. K. Mukhopadhyay, J. S. Matalobos and D. Das., *Dalton Trans.*, 2013, **42**, 16387.
- 5 Oxford Diffraction Data collection and data reduction, Version 171.34.40.
- 6 G. M. Sheldrick, *Acta Crystallogr.*, 2008, **A64**, 112.
- 7 C. Giacovazzo, *SIR-97 Program for Crystal Structure Solution*, Inst. di Ric. per lo Sviluppo di Metodologie Cristallografiche, CNR, Univ. of Bari, Italy, 1997.
- 8 I. J. Bruno, J. C. Cole, P. R. Edgington, M. Kessler, C. F. Macrae, P. McCabe, J. Pearson and R. Taylor, *Acta Crystallogr.*, 2002, **B58**, 389.



Scheme S1 Synthesis of **BAPA**, **PAPA**, **PTA** and **NBAPA**



Scheme S2 Synthesis of **BAACA** and **BANA**

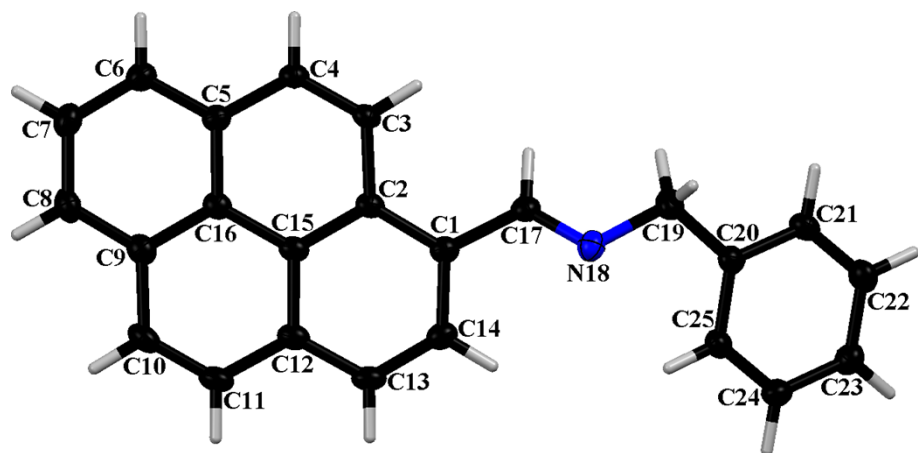


Fig. S1 Molecular structure of **BAPA**.

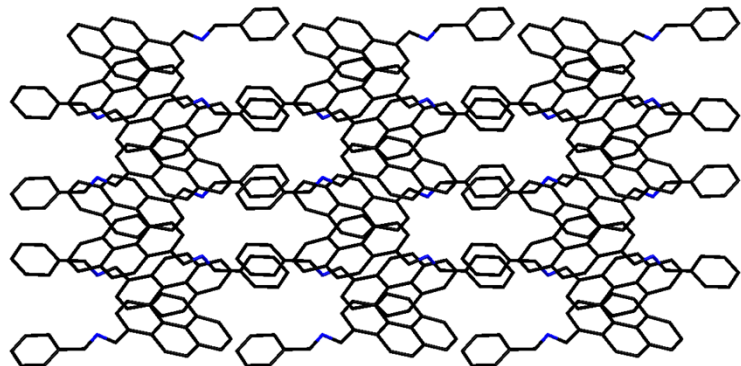
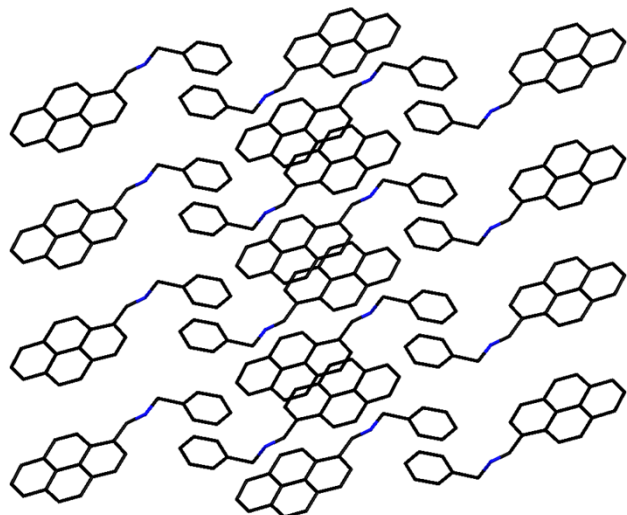
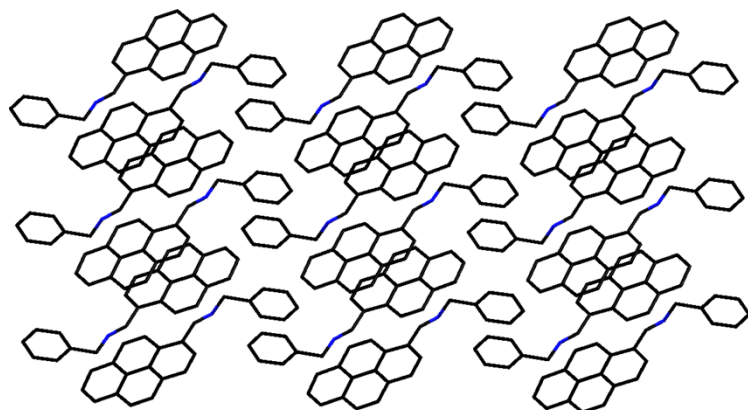


Fig. S2 Crystal packing of **BAPA** along the *a* (top), *b* (middle) and *c* (bottom) axis.

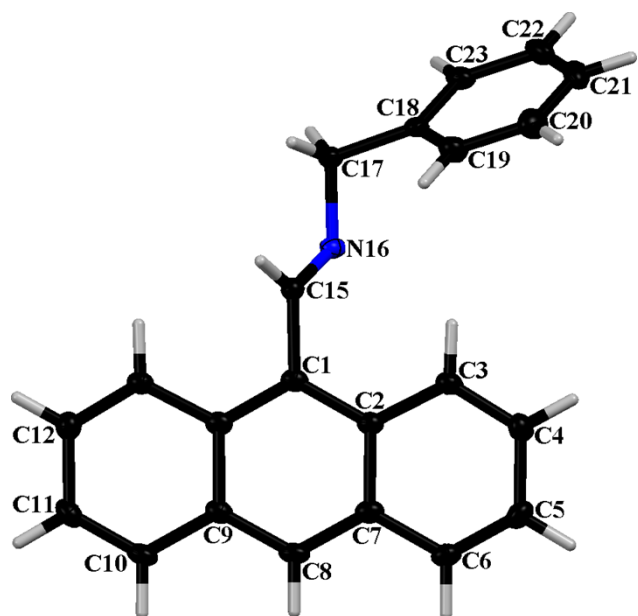


Fig. S3 Molecular structure of BAACA.

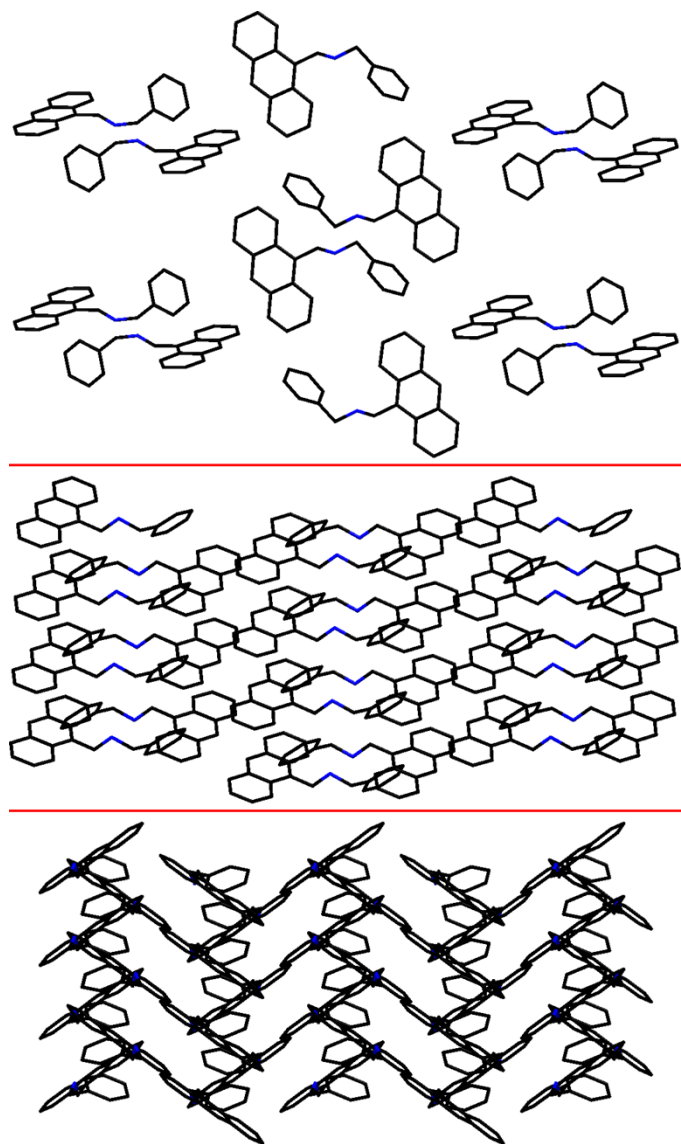


Fig. S4 Crystal packing of BAACA along the *a* (top), *b* (middle) and *c* (bottom) axis.

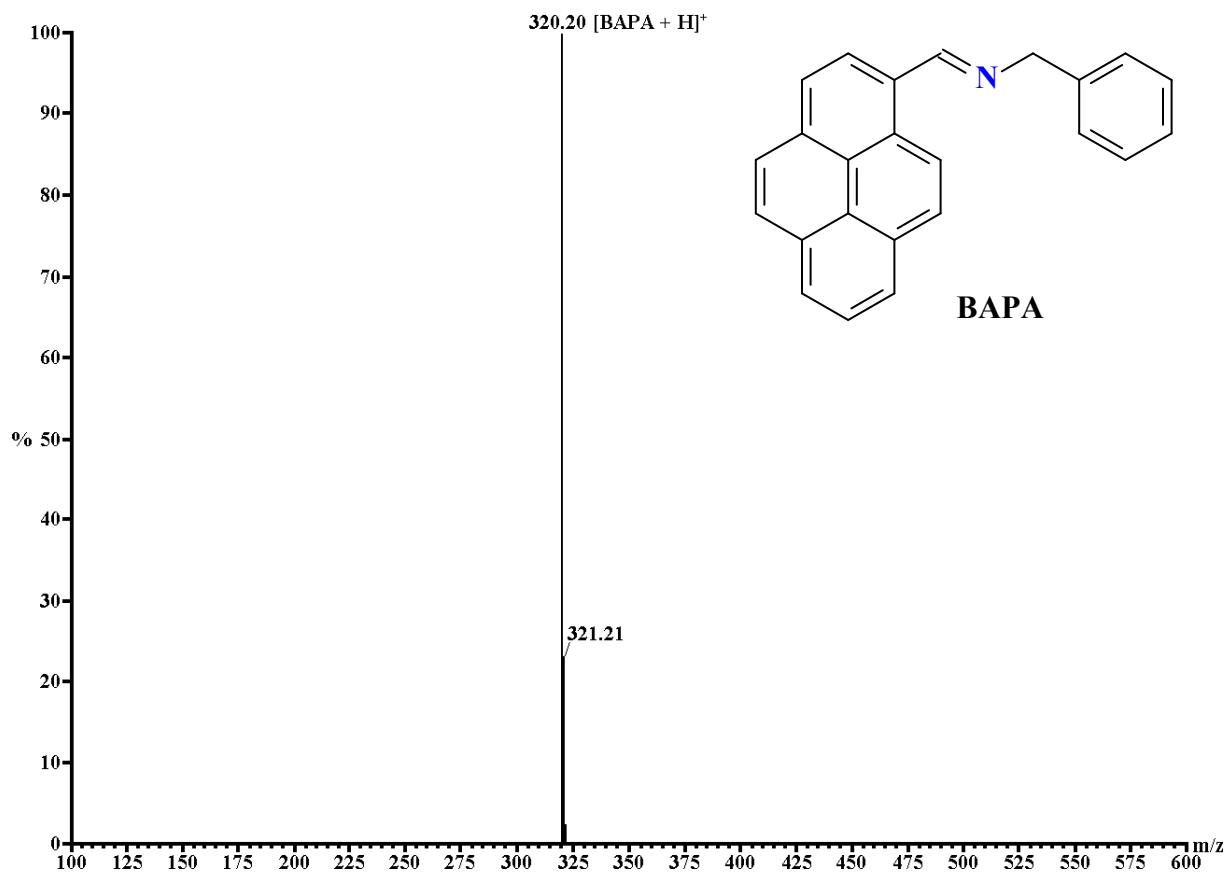


Fig. S5 The mass spectrum of **BAPA**.

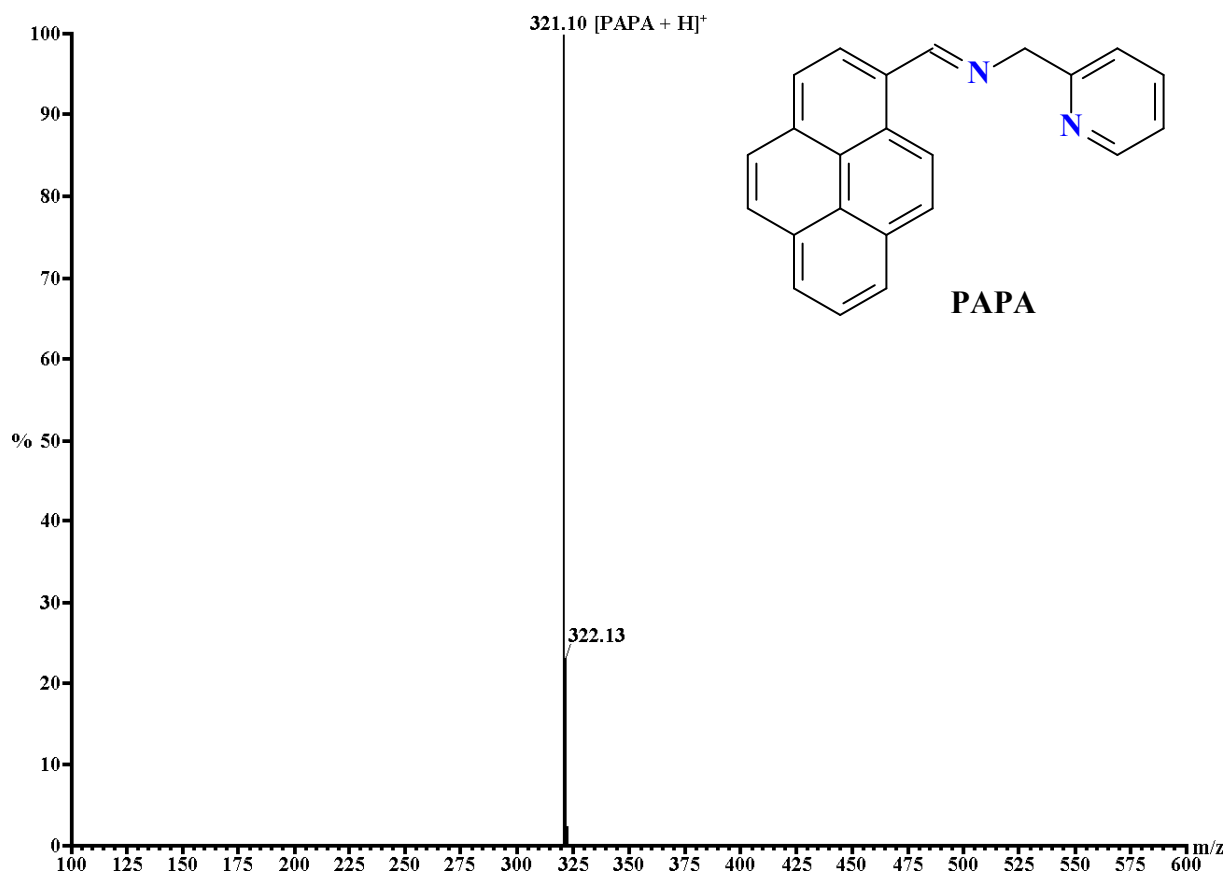


Fig. S6 The mass spectrum of **PAPA**.

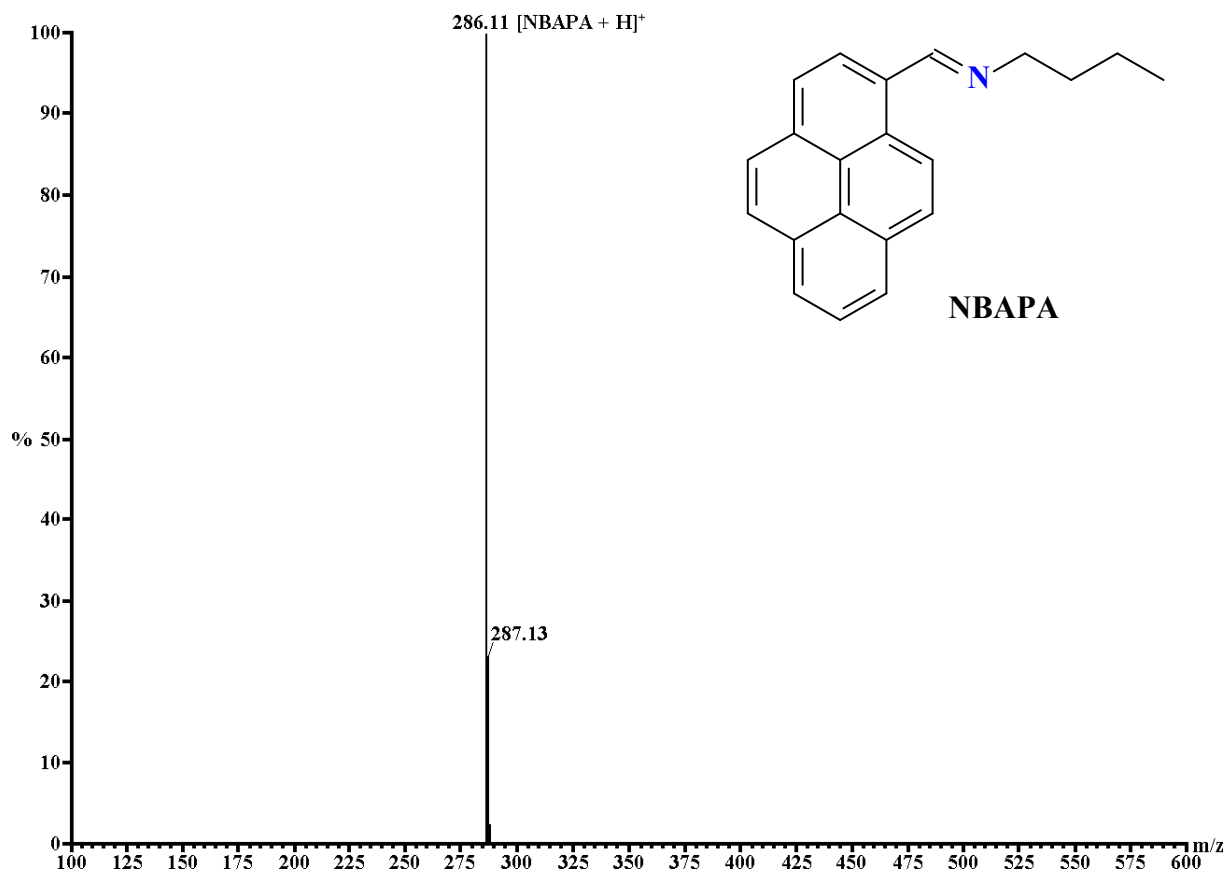


Fig. S7 The mass spectrum of NPAPA.

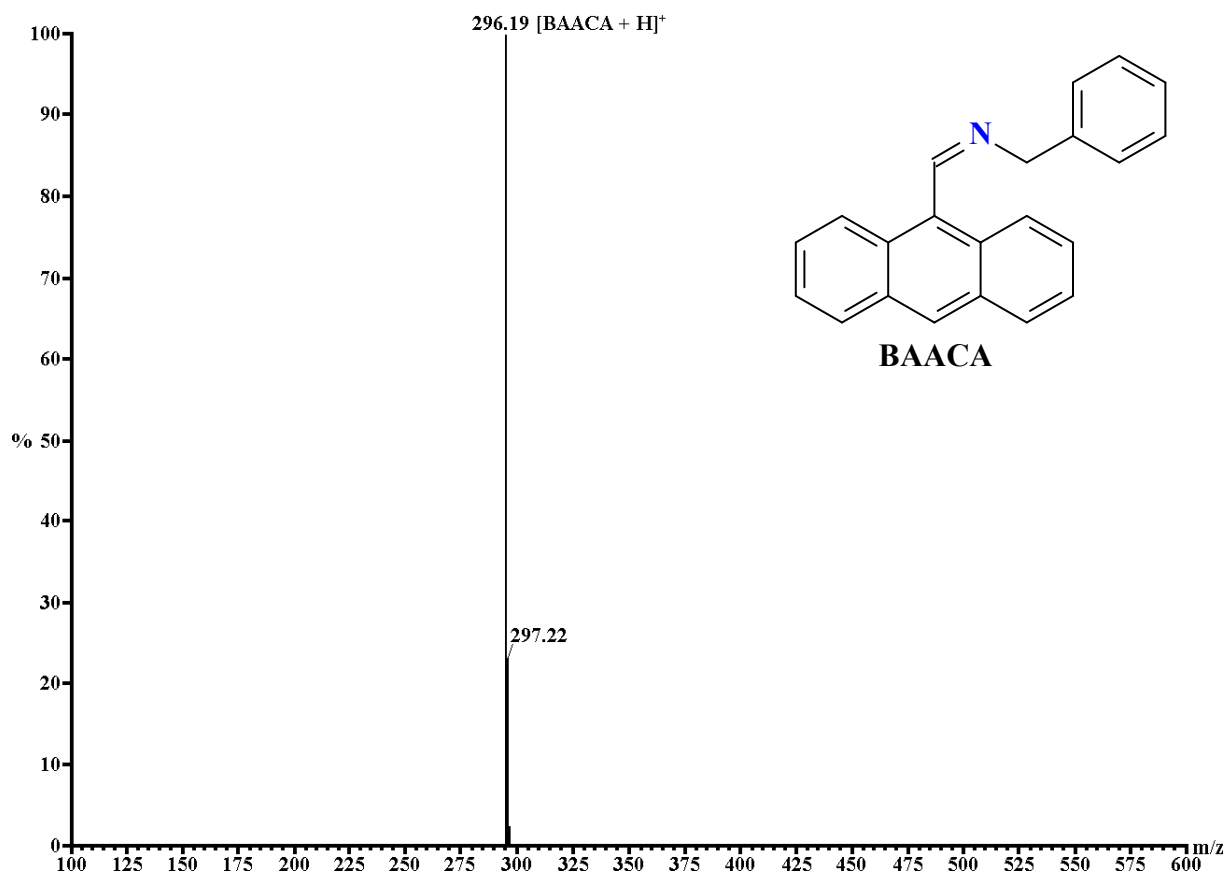


Fig. S8 The mass spectrum of BAACA.

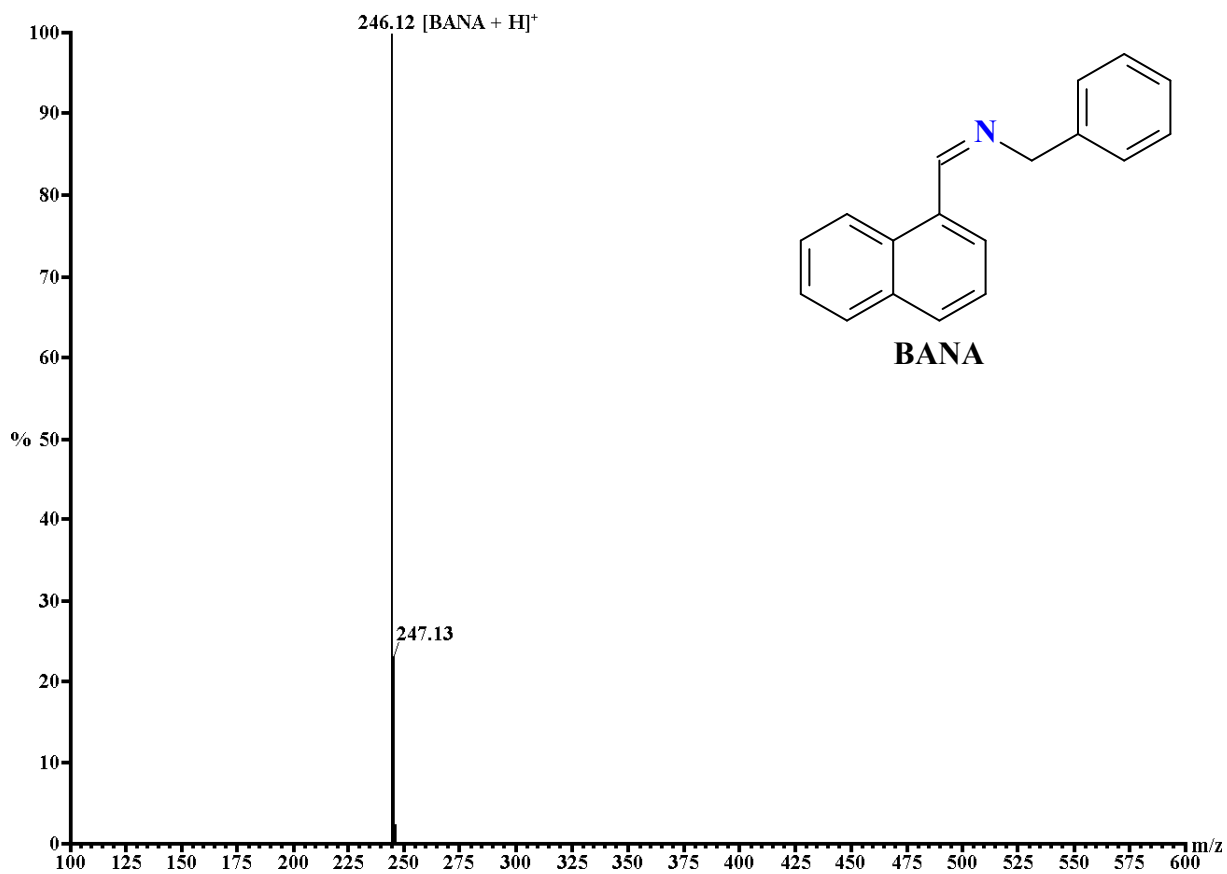


Fig. S9 The mass spectrum of BANA.

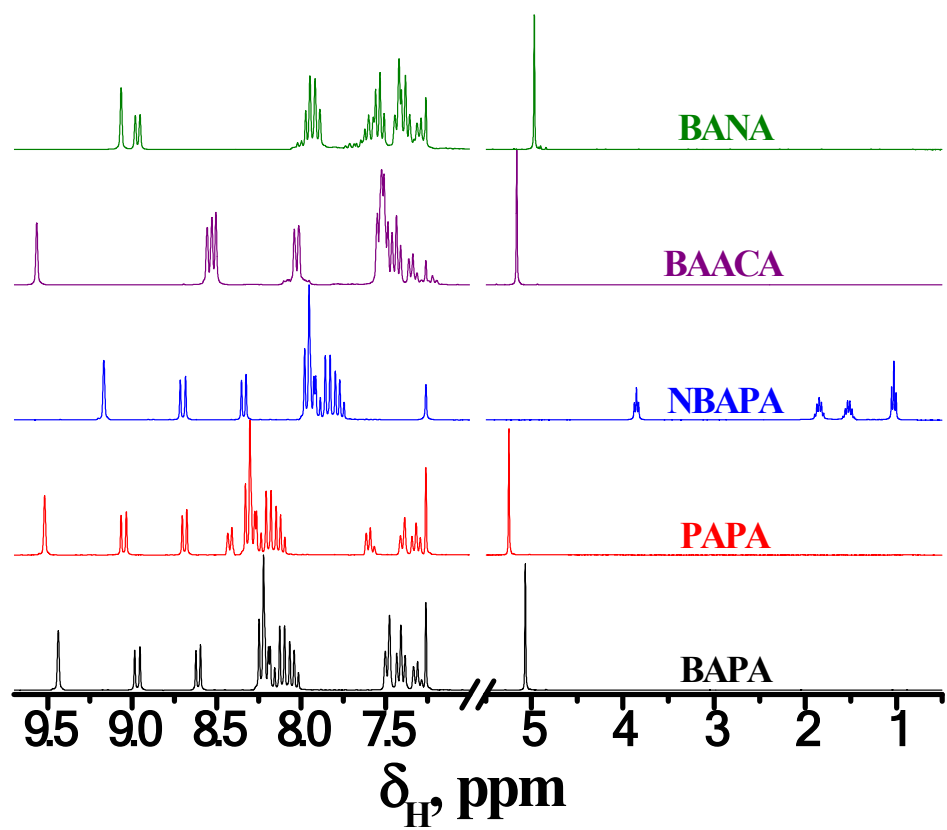


Fig. S10 The ¹H NMR spectra of BAPA, PAPA, NBAPA, BAACA and BANA.

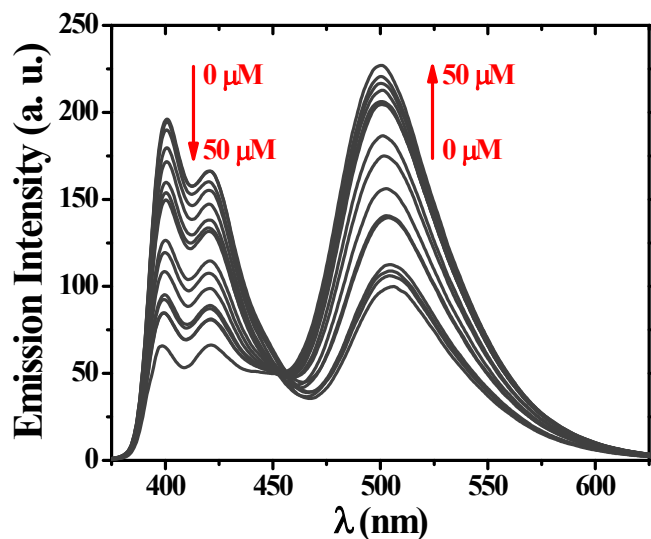


Fig. S11 Changes in the fluorescent spectra of **BAPA** (10 μM) in HEPES buffered (0.1 M; MeOH:H₂O, 1:1 v/v; pH 7.4; λ_{exc} = 360 nm) solution upon gradual addition of lysine (0, 0.005, 0.01, 0.05, 0.1, 1, 2.5, 5, 10, 15, 20, 25, 30, 35, 40, 45 and 50 μM).

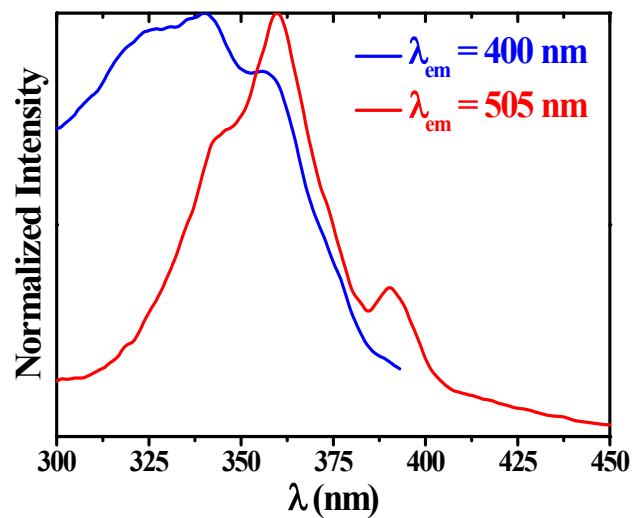
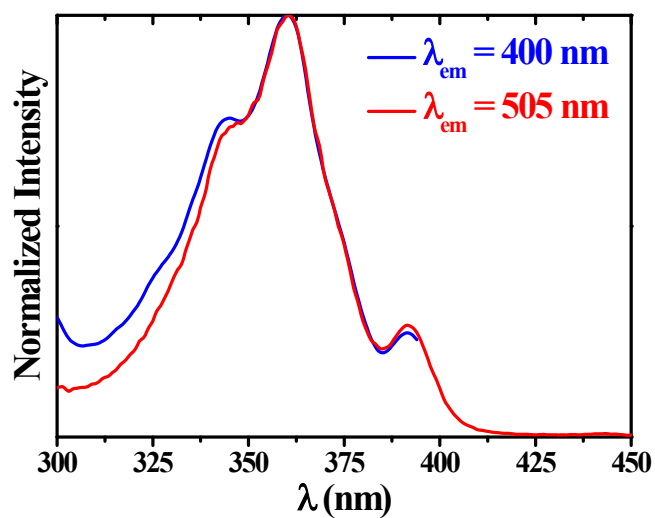


Fig. S12 Normalized excitation spectra of **BAPA** (10 μM) (left) and **BAPA** (10 μM) + 5 equivalents of lysine (right).

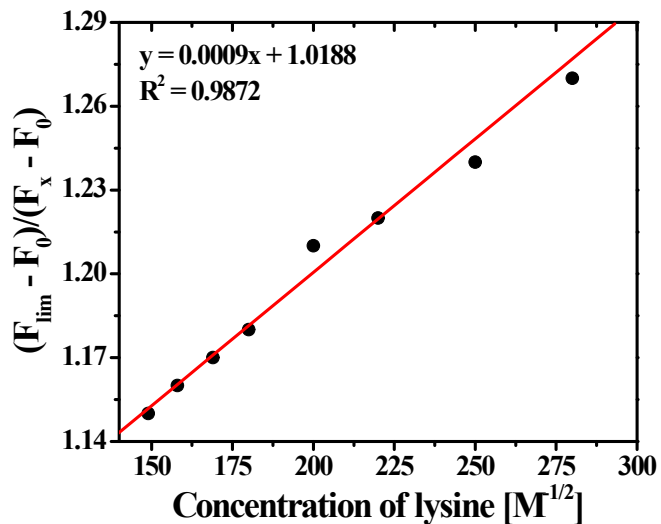


Fig. S13 The Benesi-Hildebrand plot for the determination of the association constant of **BAPA** with lysine.

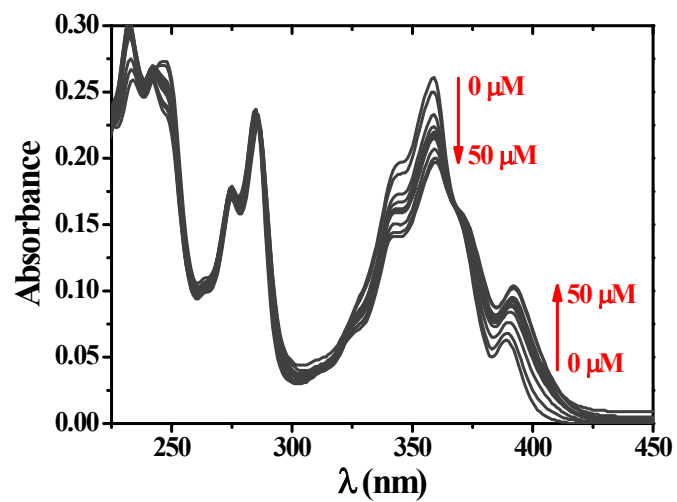


Fig. S14 Changes of absorbance of **BAPA** ($10 \mu\text{M}$) in HEPES buffered (0.1 M ; $\text{MeOH:H}_2\text{O}$, $1:1 \text{ v/v}$; $\text{pH } 7.4$) solution upon gradual addition of lysine ($0, 0.005, 0.01, 0.05, 0.1, 1, 2.5, 5, 10, 15, 20, 25, 30, 35, 40, 45$ and $50 \mu\text{M}$).

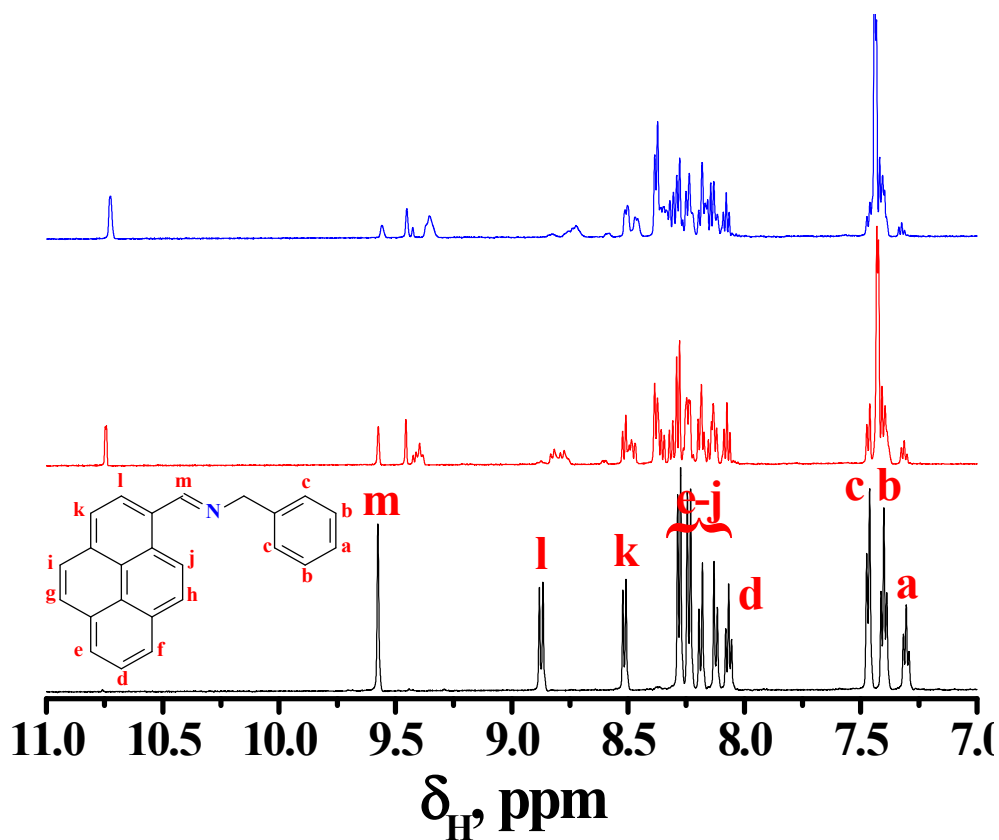


Fig. S15 ^1H NMR spectra of **BAPA** in MeOD (black), **BAPA** in MeOD + 0.5 equivalent of lysine in D_2O (red) and **BAPA** in MeOD + 1 equivalent of lysine in D_2O (blue).

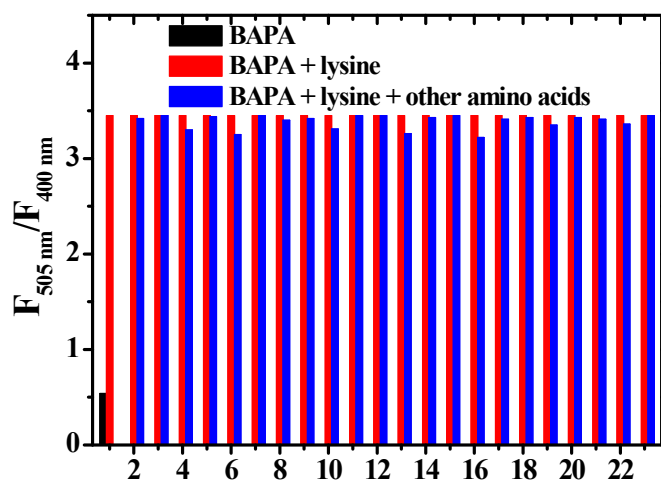


Fig. S16 Intensities ratio of the [BAPA+lysine] adduct at 505 and 400 nm in presence of different amino acids in HEPES buffered (0.1 M; MeOH:H₂O, 1:1 v/v; pH 7.4; $\lambda_{\text{exc}} = 360 \text{ nm}$) solution. Black bar: **BAPA** (10.0 μM). Red bar: **BAPA** (10.0 μM) with 5 equivalents of lysine. Blue bar: 10.0 μM of **BAPA** and 5 equivalents of lysine and 10 equivalents of amino acids (isoleucine (2), leucine(3), histidine (4), methionine (5), phenylalanine (6), threonine (7), tryptophan (8), valine(9), alanine (10), arginine (11), asparagines (12), aspartic acid (13), cysteine (14), glutamic acid (15), glutamine (16), glycine (17), ornithine (18), proline (19), serine(20), tyrosine(21) and cystine (22)).

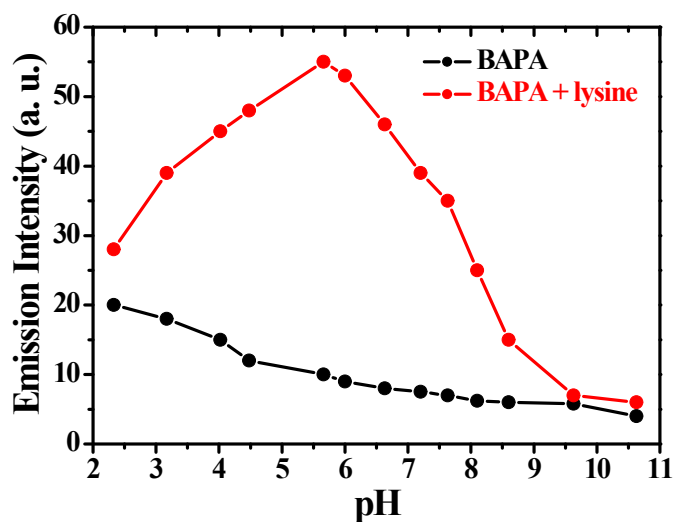


Fig. S17 Effect of pH on the emission intensities of **BAPA** (10 μM) and **BAPA** (10 μM) + 5 equivalents of lysine.

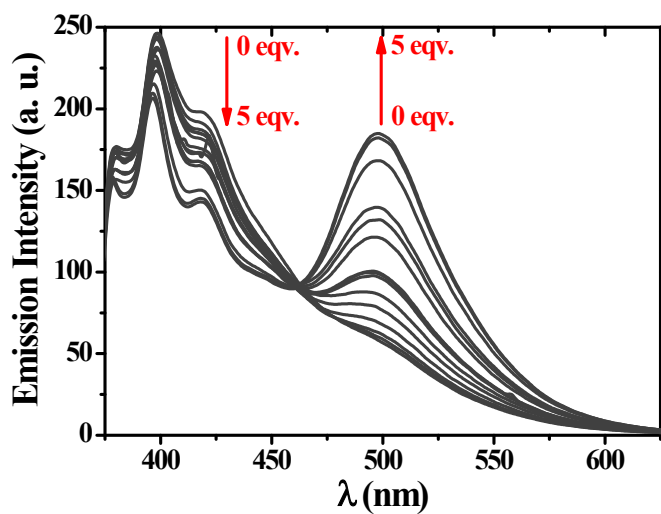


Fig. S18 Fluorescence spectra of **PAPA** (10 μM) in HEPES buffered (0.1 M; MeOH:H₂O, 1:1 v/v; pH 7.4; λ_{exc} = 345 nm) solution upon gradual addition of lysine (0, 0.01, 0.05, 0.1, 1, 2.5, 5, 10, 15, 20, 25, 30, 35, 40, 45 and 50 μM).

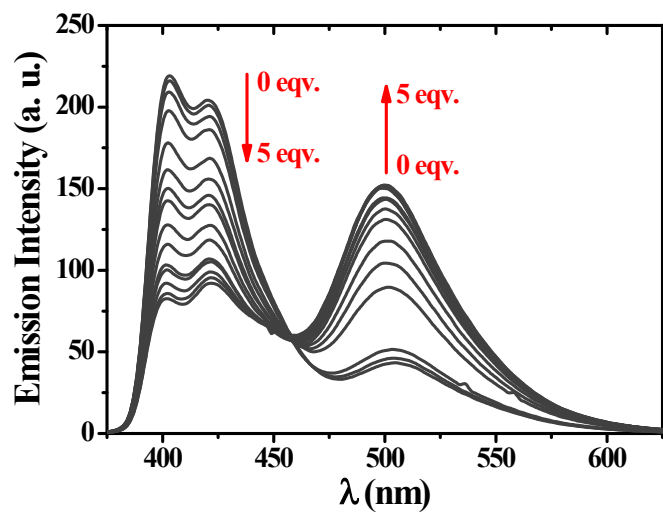


Fig. S19 Fluorescence spectra of **PTA** (10 μM) in HEPES buffered (0.1 M; MeOH:H₂O, 1:1 v/v; pH 7.4; $\lambda_{\text{exc}} = 360$ nm) solution upon gradual addition of lysine (0, 0.01, 0.05, 0.1, 1, 2.5, 5, 10, 15, 20, 25, 30, 35, 40, 45 and 50 μM).

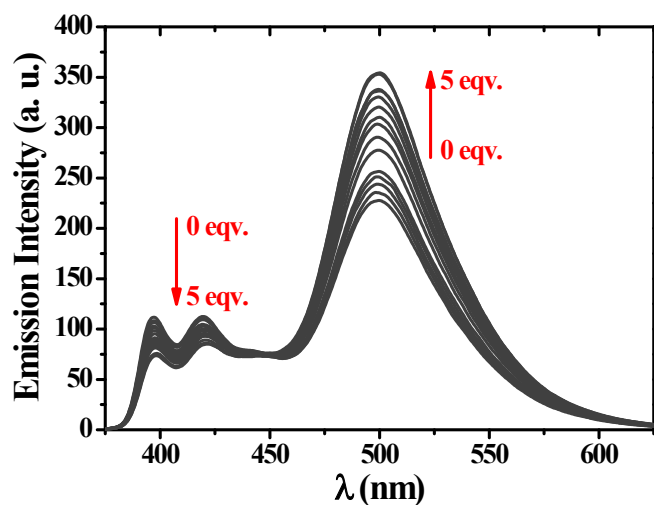


Fig. S20 Fluorescence spectra of **NBAPA** (10 μM) in HEPES buffered (0.1 M; MeOH:H₂O, 1:1 v/v; pH 7.4; $\lambda_{\text{exc}} = 360$ nm) solution upon gradual addition of lysine (0, 0.01, 0.05, 0.1, 1, 2.5, 5, 10, 15, 20, 25, 30, 35, 40, 45 and 50 μM).

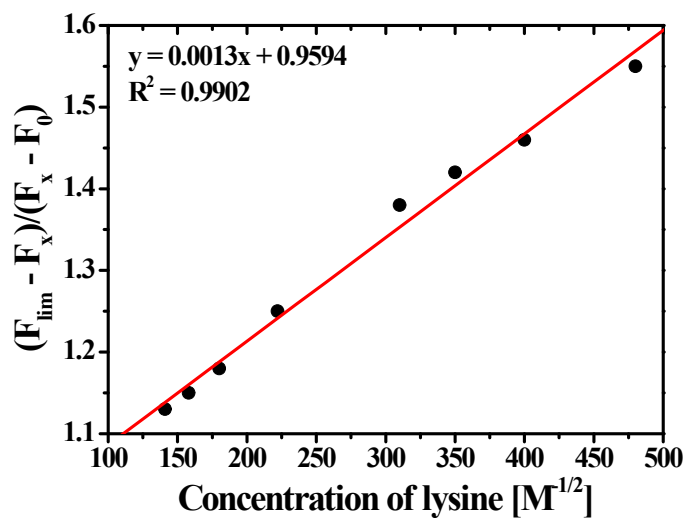


Fig. S21 The Benesi-Hildebrand plot for the determination of the association constant of **PAPA** with lysine.

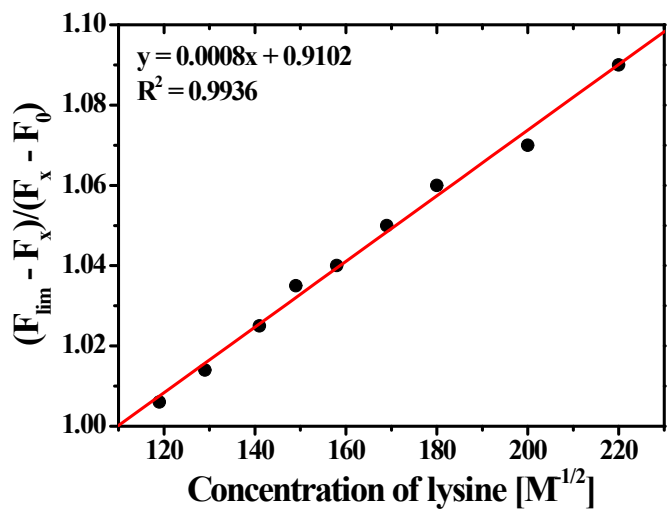


Fig. S22 The Benesi-Hildebrand plot for the determination of the association constant of **PTA** with lysine.

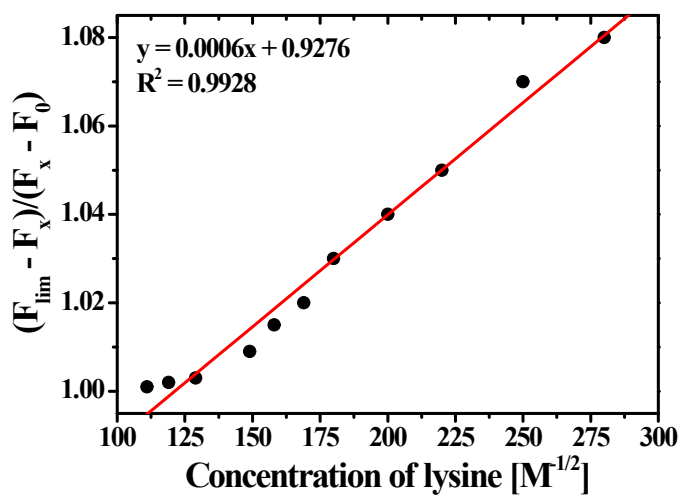


Fig. S23 The Benesi-Hildebrand plot for the determination of the association constant of **NBAPA** with lysine.

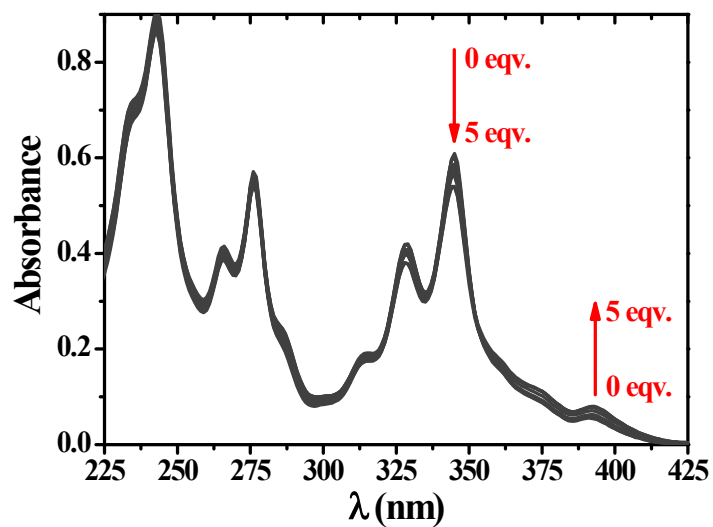


Fig. S24 Changes of absorbance of **PAPA** ($10 \mu\text{M}$) in HEPES buffered (0.1 M ; $\text{MeOH:H}_2\text{O}$, $1:1 \text{ v/v}$; $\text{pH } 7.4$) solution upon gradual addition of lysine ($0, 0.005, 0.01, 0.05, 0.1, 1, 2.5, 5, 10, 15, 20, 25, 30, 35, 40, 45$ and $50 \mu\text{M}$).

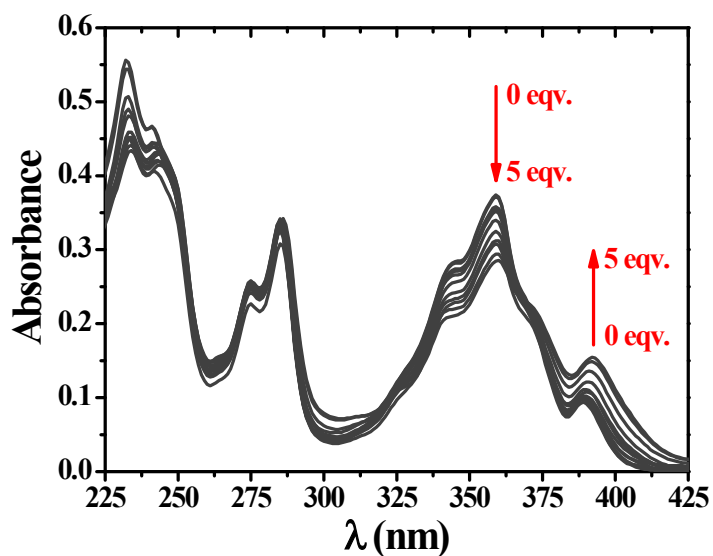


Fig. S25 Changes of absorbance of PTA (10 μM) in HEPES buffered (0.1 M; MeOH:H₂O, 1:1 v/v; pH 7.4) solution upon gradual addition of lysine (0, 0.005, 0.01, 0.05, 0.1, 1, 2.5, 5, 10, 15, 20, 25, 30, 35, 40, 45 and 50 μM).

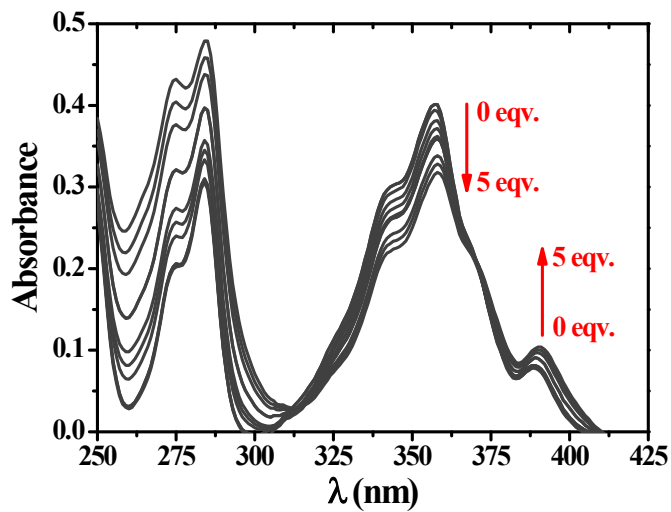


Fig. S26 Changes of absorbance of NBAPA (10 μM) in HEPES buffered (0.1 M; MeOH:H₂O, 1:1 v/v; pH 7.4) solution upon gradual addition of lysine (0, 0.005, 0.01, 0.05, 0.1, 1, 2.5, 5, 10, 15, 20, 25, 30, 35, 40, 45 and 50 μM).

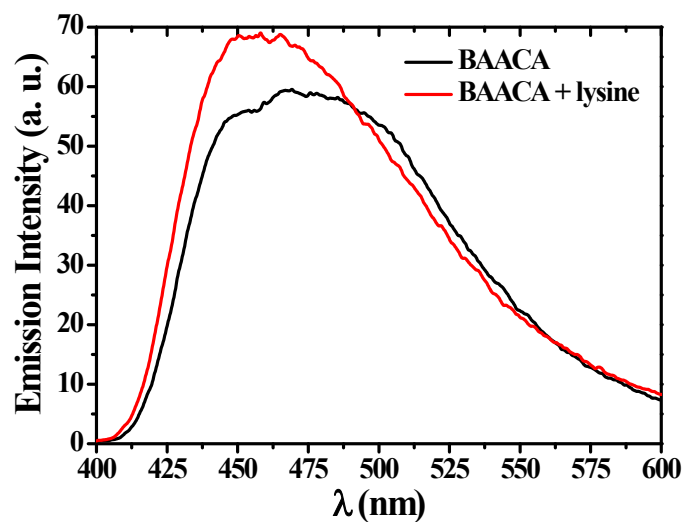


Fig. S27 Fluorescence spectra of **BAACA** and **BAACA** + 10 equivalents of lysine in HEPES buffered (0.1 M; MeOH:H₂O, 1:1 v/v; pH 7.4) solution.

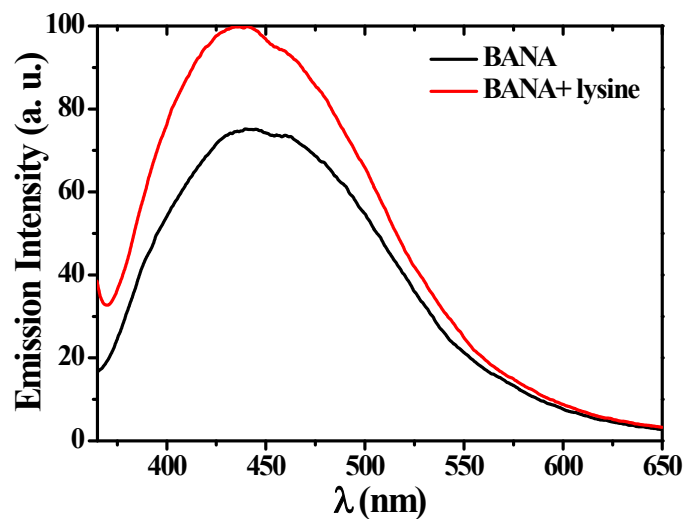


Fig. S28 Fluorescence spectra of **BANA** and **BANA** + 10 equivalents of lysine in HEPES buffered (0.1 M; MeOH:H₂O, 1:1 v/v; pH 7.4) solution.

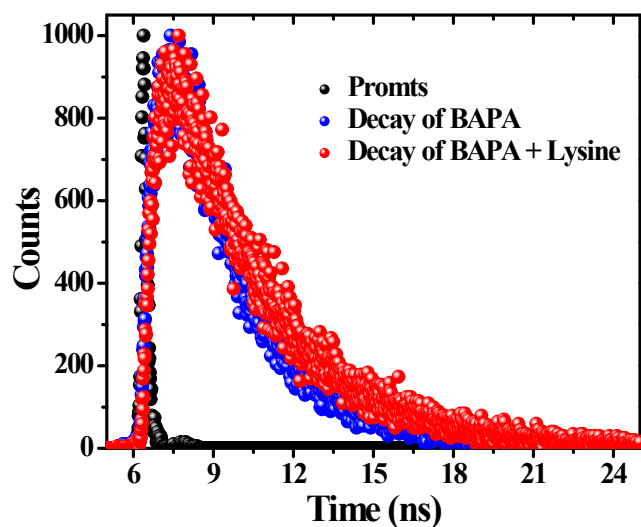


Fig. S29 Time-resolved fluorescence decay of **BAPA** (at 505 nm) in the absence and presence of lysine ($\lambda_{\text{exc}} = 360$ nm.).

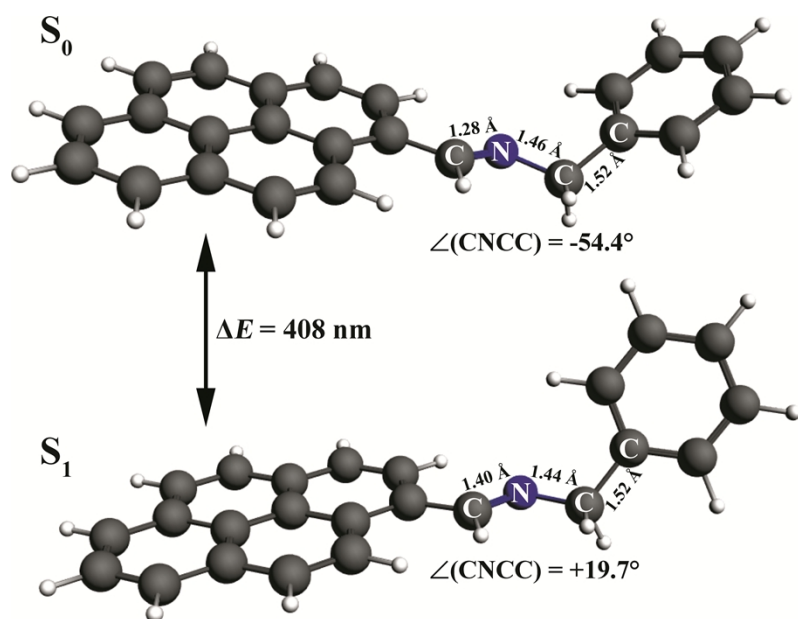
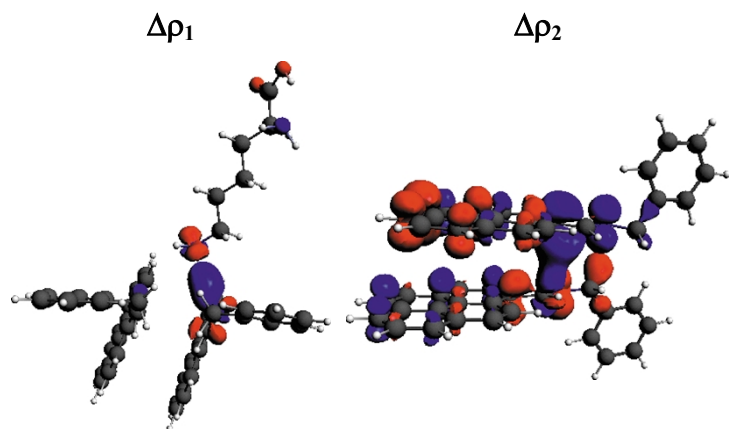


Fig. S30 Structures of the ground (S_0) and the excited (S_1) states of the **BAPA** monomer obtained from the TD-DFT (B3LYP/6-31++g**) calculations together with the differences in energy and selected geometry parameters.



$$\Delta E_{\text{orb}}(1) = -3.72 \text{ kcal/mol} \quad \Delta E_{\text{orb}}(2) = -0.73 \text{ kcal/mol}$$

Fig. S31 Leading NOCV-based deformation density channels, $\Delta\rho_1$ and $\Delta\rho_2$, with the corresponding energies, $\Delta E_{\text{orb}}(1)$ and $\Delta E_{\text{orb}}(2)$, describing the binding of neutral lysine with **BAPA dimer D (D-Lys)**.

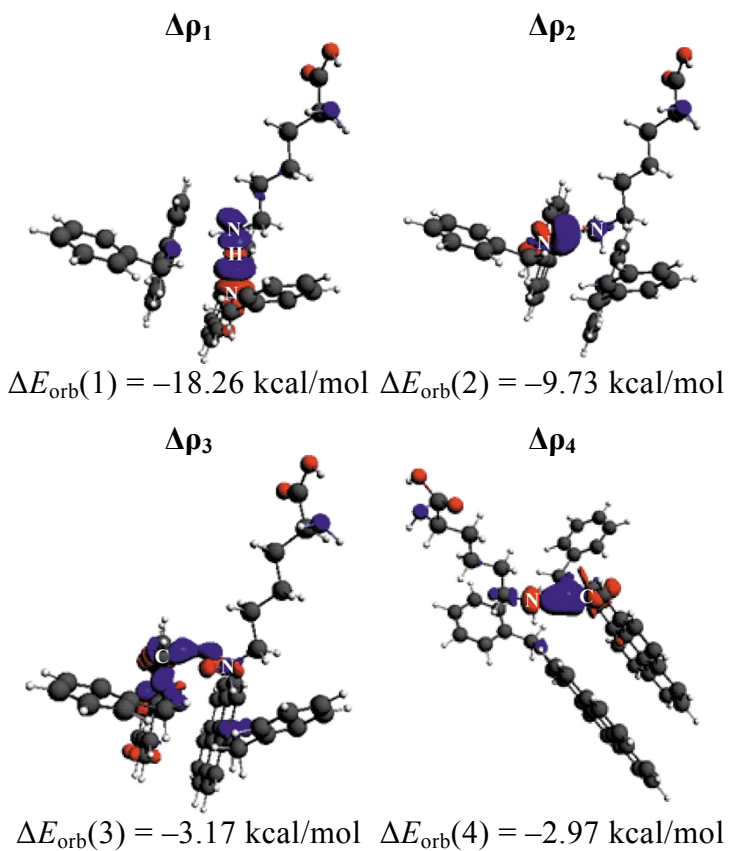


Fig. S32 The leading deformation density channels based on NOCV's, $\Delta\rho_1$, $\Delta\rho_2$, $\Delta\rho_3$, $\Delta\rho_4$, with the corresponding orbital interaction contributions $\Delta E_{\text{orb}}(1)$, $\Delta E_{\text{orb}}(2)$, $\Delta E_{\text{orb}}(3)$, $\Delta E_{\text{orb}}(4)$. The red color of $\Delta\rho_i$ shows charge depletion, whereas the blue one indicates the electron density accumulation due to formation of the **D-Lys(cationic)** complex.

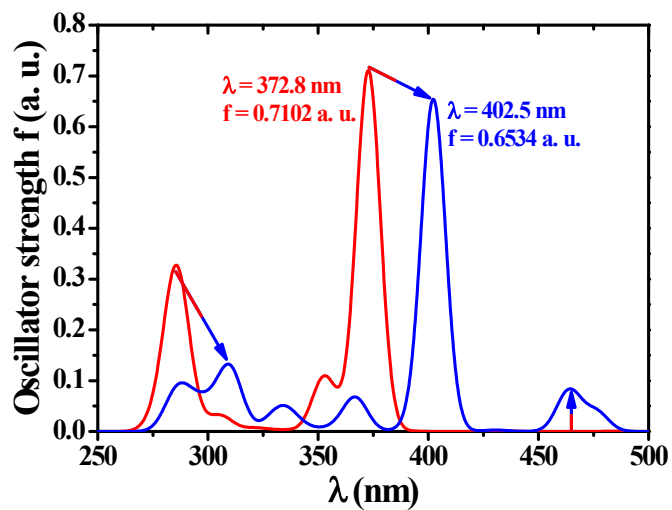


Fig. S33 The gas phase TD-DFT/B3LYP/TZP absorption spectra of **D** (red line) and **D-Lys (cationic)** (blue line). For comparison with **D-Lys (neutral)** complex see Fig. S34 in ESI†.

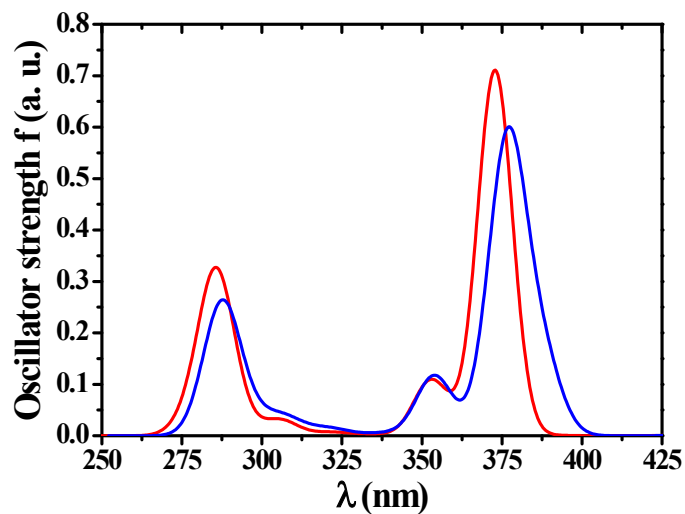


Fig. S34 The gas phase TD-DFT/B3LYP/TZP absorption spectra of **D** (red line) and **D-Lys (neutral)** (blue line).

Table S1 Selected bond lengths (Å) and bond angles (°) for **BAPA**

<i>Bond lengths</i>					
N(18)–C(17)	1.265(2)	C(5)–C(16)	1.421(3)	C(13)–C(14)	1.373(3)
N(18)–C(19)	1.459(3)	C(6)–C(7)	1.389(3)	C(15)–C(16)	1.427(3)
C(1)–C(2)	1.410(3)	C(7)–C(8)	1.382(3)	C(19)–C(20)	1.510(3)
C(1)–C(14)	1.398(3)	C(8)–C(9)	1.395(3)	C(20)–C(21)	1.386(3)
C(1)–C(17)	1.476(3)	C(9)–C(10)	1.441(3)	C(20)–C(25)	1.389(3)
C(2)–C(3)	1.442(3)	C(9)–C(16)	1.422(3)	C(21)–C(22)	1.381(3)
C(2)–C(15)	1.427(2)	C(10)–C(11)	1.344(3)	C(22)–C(23)	1.376(3)
C(3)–C(4)	1.347(3)	C(11)–C(12)	1.430(3)	C(23)–C(24)	1.372(3)
C(4)–C(5)	1.435(3)	C(12)–C(13)	1.398(3)	C(24)–C(25)	1.383(3)
C(5)–C(6)	1.394(3)	C(12)–C(15)	1.425(3)		
<i>Bond angles</i>					
C(17)–N(18)–C(19)	118.43(18)	C(7)–C(8)–C(9)	120.86(18)	C(5)–C(16)–C(9)	119.33(17)
C(2)–C(1)–C(14)	119.09(16)	C(8)–C(9)–C(10)	122.65(18)	C(5)–C(16)–C(15)	120.15(16)
C(2)–C(1)–C(17)	122.34(16)	C(8)–C(9)–C(16)	119.21(17)	C(9)–C(16)–C(15)	120.51(16)
C(14)–C(1)–C(17)	118.51(16)	C(10)–C(9)–C(16)	118.12(17)	N(18)–C(17)–C(1)	121.29(17)
C(1)–C(2)–C(3)	123.20(16)	C(9)–C(10)–C(11)	121.48(18)	N(18)–C(19)–C(20)	111.60(17)
C(1)–C(2)–C(15)	119.27(16)	C(10)–C(11)–C(12)	121.66(18)	C(19)–C(20)–C(21)	119.38(18)
C(3)–C(2)–C(15)	117.52(16)	C(11)–C(12)–C(13)	122.46(17)	C(19)–C(20)–C(25)	122.52(18)
C(2)–C(3)–C(4)	121.71(17)	C(11)–C(12)–C(15)	118.88(17)	C(21)–C(20)–C(25)	118.09(18)
C(3)–C(4)–C(5)	122.04(17)	C(13)–C(12)–C(15)	118.63(17)	C(20)–C(21)–C(22)	120.95(18)
C(4)–C(5)–C(6)	122.42(17)	C(12)–C(13)–C(14)	120.92(17)	C(21)–C(22)–C(23)	120.32(19)
C(4)–C(5)–C(16)	118.02(16)	C(1)–C(14)–C(13)	121.98(17)	C(22)–C(23)–C(24)	119.47(19)
C(6)–C(5)–C(16)	119.51(16)	C(2)–C(15)–C(12)	120.11(16)	C(23)–C(24)–C(25)	120.47(18)
C(5)–C(6)–C(7)	120.46(17)	C(2)–C(15)–C(16)	120.54(16)	C(20)–C(25)–C(24)	120.71(18)
C(6)–C(7)–C(8)	120.60(18)	C(12)–C(15)–C(16)	119.32(16)		

Table S2 Selected bond lengths (Å) and bond angles (°) for **BAACA**

<i>Bond lengths</i>					
N(16)–C(15)	1.2712(17)	C(5)–C(6)	1.356(2)	C(13)–C(14)	1.430(2)
N(16)–C(17)	1.4710(17)	C(6)–C(7)	1.428(2)	C(17)–C(18)	1.510(2)
C(1)–C(2)	1.410(2)	C(7)–C(8)	1.3935(19)	C(18)–C(19)	1.394(2)
C(1)–C(14)	1.4114(19)	C(8)–C(9)	1.390(2)	C(18)–C(23)	1.385(2)
C(1)–C(15)	1.4827(19)	C(9)–C(10)	1.4271(19)	C(19)–C(20)	1.382(2)
C(2)–C(3)	1.4325(19)	C(9)–C(14)	1.4359(19)	C(20)–C(21)	1.385(2)
C(2)–C(7)	1.4380(19)	C(10)–C(11)	1.358(2)	C(21)–C(22)	1.382(3)
C(3)–C(4)	1.362(2)	C(11)–C(12)	1.420(2)	C(22)–C(23)	1.390(2)
C(4)–C(5)	1.419(2)	C(12)–C(13)	1.360(2)		
<i>Bond angles</i>					
C(15)–N(16)–C(17)	116.74(12)	C(2)–C(7)–C(8)	119.50(12)	C(9)–C(14)–C(13)	117.72(12)
C(2)–C(1)–C(14)	120.42(12)	C(6)–C(7)–C(8)	121.27(12)	N(16)–C(15)–C(1)	121.88(12)
C(2)–C(1)–C(15)	120.99(12)	C(7)–C(8)–C(9)	121.84(12)	N(16)–C(17)–C(18)	109.10(11)
C(14)–C(1)–C(15)	118.55(12)	C(8)–C(9)–C(10)	121.55(12)	C(17)–C(18)–C(19)	119.37(12)
C(1)–C(2)–C(3)	123.21(12)	C(8)–C(9)–C(14)	119.30(12)	C(17)–C(18)–C(23)	121.92(13)
C(1)–C(2)–C(7)	119.29(12)	C(10)–C(9)–C(14)	119.14(12)	C(19)–C(18)–C(23)	118.70(13)
C(3)–C(2)–C(7)	117.48(12)	C(9)–C(10)–C(11)	121.00(13)	C(18)–C(19)–C(20)	120.59(14)
C(2)–C(3)–C(4)	121.04(12)	C(10)–C(11)–C(12)	120.17(14)	C(19)–C(20)–C(21)	120.29(15)
C(3)–C(4)–C(5)	121.20(14)	C(11)–C(12)–C(13)	120.66(13)	C(20)–C(21)–C(22)	119.68(15)
C(4)–C(5)–C(6)	119.73(14)	C(12)–C(13)–C(14)	121.30(12)	C(21)–C(22)–C(23)	119.96(15)
C(5)–C(6)–C(7)	121.29(14)	C(1)–C(14)–C(9)	119.64(12)	C(18)–C(23)–C(22)	120.78(14)
C(2)–C(7)–C(6)	119.23(12)	C(1)–C(14)–C(13)	122.62(12)		

Table S3 The ETS energy decomposition results, describing the bonding in **D** and **D-Lys**

BLYP-D3/TZ2P	D^a	D-Lys(neutral)^a	D-Lys(cationic)^a
$\Delta E_{\text{total}}^b$	-17.79	-9.41	-63.65
ΔE_{orb}	-4.46	-5.98	-56.04
ΔE_{elstat}	-9.50	-11.39	-51.62
ΔE_{Pauli}	25.74	17.09	60.97
$\Delta E_{\text{dispersion}}$	-29.57	-9.13	-16.95

^a Values are in kcal/mol. ^b $\Delta E_{\text{total}} = \Delta E_{\text{orb}} + \Delta E_{\text{elstat}} + \Delta E_{\text{Pauli}} + \Delta E_{\text{dispersion}}$